

Motility-Induced Phase Separation Mediated by Bacterial Quorum Sensing

Wesley J. M. Ridgway^{1,*}, Mohit P. Dalwadi^{1,2,3,†}, Philip Pearce^{1,2,3,‡} and S. Jonathan Chapman^{1,§}

¹Mathematical Institute, University of Oxford, Oxford OX2 6GG, United Kingdom

²Department of Mathematics, University College London, London WC1H 0AY, United Kingdom

³Institute for the Physics of Living Systems, University College London, London, United Kingdom



(Received 3 April 2023; accepted 9 October 2023; published 30 November 2023)

We study motility-induced phase separation (MIPS) in living active matter, in which cells interact through chemical signaling, or quorum sensing. In contrast to previous theories of MIPS, our multiscale continuum model accounts explicitly for genetic regulation of signal production and motility. Through analysis and simulations, we derive a new criterion for the onset of MIPS that depends on features of the genetic network. Furthermore, we identify and characterize a new type of oscillatory instability that occurs when gene regulation inside cells promotes motility in higher signal concentrations.

DOI: [10.1103/PhysRevLett.131.228302](https://doi.org/10.1103/PhysRevLett.131.228302)

Introduction.—Chemical signals control cell motility to regulate self-organized patterning in living systems, from tissue morphogenesis and wound healing to cancer [1]. In bacterial populations, chemical signaling, or quorum sensing (QS), drives self-organization by promoting population-level behaviors such as biofilm formation and swarming motility [2,3]. Bacterial QS systems have been engineered to connect directly to genes controlling motility in synthetic genetic networks, enabling the generation of tunable patterns *in vitro* [4–6]. However, we lack fundamental understanding of how cell-level features, such as gene-regulatory networks, determine emergent population-level pattern formation in living active matter.

Minimal physical models of active and living matter typically consist of physically interacting self-propelled particles. Despite their simplicity, such models can display complex emergent dynamics, such as motility-induced phase separation (MIPS) [7,8]. This phenomenon is caused by a self-trapping mechanism whereby particles experience reduced motility at high densities owing to their interactions, eventually leading to dense macroscopic clusters of immotile particles coexisting with a dilute phase of motile particles [7]. Similar phase transitions have been observed in active matter systems with agents that interact through flows [9–13], morphogens [14], social interactions [15,16], chemotaxis [17–21], and electrostatic torques [22]. In the past, models for chemically interacting particles have been placed within this framework by representing signals indirectly through a density-dependent motility [7,23–25]

or an effective physical force [26,27], but it is not known how far these approaches accurately represent chemical signaling in living matter.

More recently, minimal models of active matter have been supplemented with a concentration field of signaling molecules that mediates the orientation [21,28–34] or motility [5,35–37] of cells or particles. Such models have demonstrated that, broadly, repression of motility by intercellular signals tends to promote variations in cell density [5,36,38–41], in line with models of physically interacting particles. However, these existing models often represent gene regulation and chemical signaling using coarse-grained or effective terms, rather than accounting for gene-regulatory kinetics explicitly. Therefore, it is not known in general how the properties of gene-regulatory networks connect to the characteristics of emergent patterns in living active matter.

Here, we develop a multiscale continuum model of chemically interacting particles or cells. Our theory systematically accounts for intracellular processes through careful treatment of the population’s gene regulation and phenotype (i.e., motility). Thereby, we connect population-level patterns with the gene-regulatory network inside cells and intercellular QS signaling. We derive a criterion for MIPS mediated by QS in terms of the properties of the gene-regulatory network and discover a new route to MIPS via genetic regulation of tumbling frequency. We clarify that it is only consistent to approximate chemically mediated interactions by a density-dependent motility in the limit of fast chemical timescales; in general, one must account for chemical timescales to predict the onset of QS-induced MIPS. Moreover, the density dependence we derive is nonlinear, in contrast to physically interacting active Brownian particles (ABPs) [42–44]. Finally, we identify and explain a new type of oscillatory instability that occurs when cell motility is promoted, rather than

Published by the American Physical Society under the terms of the [Creative Commons Attribution 4.0 International license](https://creativecommons.org/licenses/by/4.0/). Further distribution of this work must maintain attribution to the author(s) and the published article’s title, journal citation, and DOI.

repressed, in higher concentrations of QS signal. This new instability does not occur in active matter systems in which the interactions are purely physical.

Model setup.—We start by imposing rules at the cell level, before systematically deriving a continuum model from the cell dynamics. We consider a population of N chemically interacting bacteria in two dimensions, and neglect physical interactions to focus on the role of chemical signaling.

Each cell is denoted by the index i and is located at position \mathbf{x}_i with an internal chemical concentration $u_i(t)$, which represents a gene-regulatory protein or transcription factor. The internal chemical obeys the kinetics

$$\dot{u}_i = f[u_i, c(\mathbf{x}_i, t)] + \sqrt{2\varepsilon}\xi_i(t). \quad (1)$$

Here, f characterizes the gene-regulatory network (GRN), and depends on the internal chemical concentration u_i and the local concentration field c of autoinducer (AI), which permeates the population. Although our upscaling is general, we later define f for definiteness. The last term in (1) represents the stochastic behaviour inherent to chemical reactions; ξ_i represents zero-mean Gaussian white noise and ε its magnitude. We work in the limit of small magnitude noise in the gene-regulatory kinetics. We include this small noise term for two reasons. First, biochemical reactions are intrinsically stochastic, especially if the reagents are present in small amounts [45]. Second, this term regularizes the continuum equations and, as we show below, the system is singular in the limit $\varepsilon \rightarrow 0$.

In terms of cell motility, we assume that the cells undergo both active motion and passive diffusion. The active component is characterized by active Brownian motion [46,47] and run-and-tumble dynamics. Between tumbles, the particle positions \mathbf{x}_i therefore obey

$$\dot{\mathbf{x}}_i = v(u_i)\mathbf{e}_i + \sqrt{2D_t}\zeta_i(t), \quad (2)$$

where $v(u_i)$ is the gene-regulated self-propulsion speed and D_t a passive translational diffusion coefficient associated with the zero-mean Gaussian white noise ζ_i . The cell orientations are described by the vector $\mathbf{e}_i = (\cos\phi_i, \sin\phi_i)^T$, where the angle ϕ_i undergoes diffusion with no directional bias due to the active Brownian component:

$$\dot{\phi}_i = \sqrt{2D_r(u_i)}\eta_i(t), \quad (3)$$

where D_r is a rotational diffusion coefficient associated with the zero-mean Gaussian white noise η_i . The active motility parameters D_r , v , and the tumble rate γ are gene-regulated, which is modeled by allowing a dependence on u_i . Such regulation may arise naturally [3,48] or synthetically [4–6].

We derive continuum equations from the individual-based equations of motion (1)–(3) for a large population

of cells using standard methods (see Sec. A of the Supplemental Material [49], cf. [44,53–55]). In the continuum equations, the intracellular chemical concentration u becomes an independent variable. That is, the population-level equations are structured in terms of the GRN inside cells; we refer to these multiscale equations as GRN structured.

The continuum GRN-structured cell density $n(\mathbf{x}, u, t)$ satisfies

$$\partial_t n = \mathcal{D}(u)\nabla^2 n + \varepsilon\partial_u^2 n - \partial_u(f(u, c)n), \quad (4a)$$

$$\mathcal{D}(u) := D_t + \frac{v^2(u)}{2[\gamma(u) + D_r(u)]}. \quad (4b)$$

Here, $\mathcal{D}(u)$ is the effective gene-regulated diffusion coefficient, and ∇ refers to spatial derivatives. The second term on the rhs of (4a) accounts for the stochastic component of the kinetics. The third term on the rhs of (4a) codifies the GRN through an advection of the structured cell density in the u coordinate. The second term on the rhs of (4b) is the contribution arising from the run-and-tumble and active Brownian dynamics. The physical cell density $\rho(\mathbf{x}, t)$ is related to the GRN-structured cell density n through $\rho = \int_0^\infty n du$. In deriving Eqs. (4), we assume that the gene-regulatory kinetics and cell diffusion occur on timescales much longer than the tumbling and reorientation timescales, in line with biological parameter estimates [36,56], and consider length scales much larger than the cell persistence length (see Sec. A of the Supplemental Material [49]).

Positive feedback is a canonical component of quorum-sensing GRNs, present in many bacterial species [2,56]. We pose the following specific functional form for f which incorporates positive feedback:

$$f(u, c) = a + \frac{Lc}{K+c} - \lambda u. \quad (5)$$

Here, a represents a constant base production rate of the intracellular chemical u , and λ is a natural decay rate. The second term on the rhs of (5) represents the production of u induced by the local AI concentration c , which constitutes one half of the positive feedback loop illustrated in Fig. 1(a). This term saturates at a maximal rate of L and has a “threshold” activation at $c = K$ where the production rate is half-maximal.

The other half of the positive feedback loop in the QS circuit involves the AI concentration field $c(\mathbf{x}, t)$. We assume that AI diffuses passively with coefficient D_c , decays with rate β , and is generated through cell secretion at a rate $\alpha(u)$. Thus, we have

$$\partial_t c = D_c\nabla^2 c - \beta c + \int_0^\infty \alpha(u)n(\mathbf{x}, u, t)du, \quad (6)$$

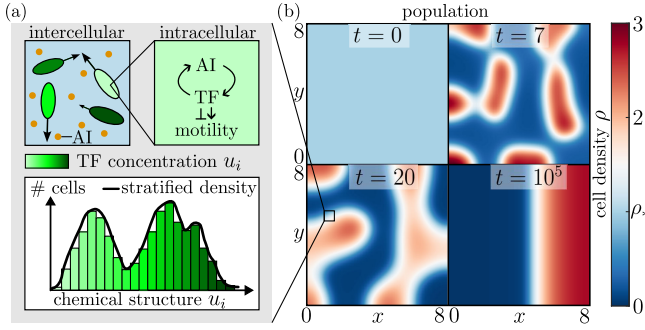


FIG. 1. (a) Schematic illustration of our multiscale model of chemically interacting cells. We derive a continuum population model that retains the genetic structure of the population through chemical stratification. The motility of individual cells depends on their internal chemical concentration. The transcription factor can either repress or promote motility. (b) Snapshots in time of the cell density from an initially homogeneous state (AI concentration profile is similar). See also video S1 in the Supplemental Material [49].

where the final term on the rhs is the continuum secretion term. This term is nonlocal in u as it encodes the contribution from all internal concentrations in a locally averaged region of space. We emphasize that positive feedback is only present in the QS circuit when the secretion rate $\alpha(u)$ is nonconstant across internal concentrations u . For simplicity, we pose a secretion rate that is proportional to the internal concentration, i.e.,

$$\alpha(u) = \alpha_0 u. \quad (7)$$

Finally, we assume that the cell population and concentration field are confined to a rectangular domain Ω , imposing no flux boundary conditions on the boundaries $\partial\Omega$. Hence,

$$\nabla n \cdot \mathbf{N} = 0, \quad \nabla c \cdot \mathbf{N} = 0, \quad \mathbf{x} \in \partial\Omega, \quad (8)$$

where \mathbf{N} is the unit normal on $\partial\Omega$. To ensure physical (i.e., non-negative, bounded) concentrations, we also impose no flux at $u = 0$ and as $u \rightarrow \infty$. These conditions correspond to

$$\varepsilon \partial_u n - f(u, c)n = 0, \quad \text{for } u = 0, u \rightarrow \infty. \quad (9)$$

Our continuum model therefore consists of the governing equations (4)–(7), and the boundary conditions (8) and (9). The multiscale nature of our model is illustrated schematically in Fig. 1(a). We verify the predictions of our theory in the following section via numerical simulations of the governing equations, using the open-source finite-element library oomph-lib [57] (see Sec. E of the Supplemental Material [49]).

Instability of the uniform equilibrium state.—To investigate the emergence of MIPS in our model, we search for instabilities in the *spatially* uniform equilibrium state,

emphasizing that this is not *chemically* uniform in general. To this end, we perform a linear stability analysis of the governing equations (4)–(9) to derive an instability criterion for the onset of MIPS.

We derive the steady uniform solution by directly integrating (4a) and imposing the boundary conditions (9). The spatially uniform equilibrium is then given by

$$c_* = \text{const}, \quad n_e(u) = \rho_* \sqrt{\frac{\lambda}{2\pi\varepsilon}} \exp\left[-\frac{\lambda}{2\varepsilon}(u - u_*)^2\right], \quad (10)$$

where the steady AI concentration c_* and mean internal concentration u_* are defined through the unique positive solution of the algebraic system

$$f(u_*, c_*) = 0, \quad \beta c_* = \alpha_0 \rho_* u_*, \quad (11)$$

where $\rho_* := \int_0^\infty n_e du$ represents the uniform cell density.

The analysis is singular in the limit $\varepsilon \rightarrow 0$, since the equilibrium density n_e (10) formally tends to a Dirac delta function centred at $u = u_*$, representing identical internal concentrations in each cell. To analyze this singular perturbation problem, we perform a WKBJ-like asymptotic approximation and explicitly factor out the singular exponential term. This reduces the analysis to a regular perturbation problem (see Sec. B of the Supplemental Material [49]).

We perform the linear stability analysis by substituting small perturbations of the form

$$n(\mathbf{x}, u, t) = n_e(u) + \eta(u) e^{i\mathbf{k} \cdot \mathbf{x} + \sigma t}, \quad c(\mathbf{x}, t) = c_* + C e^{i\mathbf{k} \cdot \mathbf{x} + \sigma t}, \quad (12)$$

into the governing equations (4)–(6) and linearizing the result. Here, \mathbf{k} denotes the wavenumber and σ the growth rate of the small perturbations. This yields the dispersion relation (see Sec. B of the Supplemental Material [49])

$$\sigma + D_c k^2 + \beta - \alpha_0 f_c^* \rho_* \frac{\sigma + (D_* - D'_* u_*) k^2}{(\sigma + D_* k^2)(\sigma + D_* k^2 + \lambda)} = 0. \quad (13)$$

Here $k := |\mathbf{k}|$ while $D_* := D(u_*)$, $D'_* := D'(u_*)$, and $f_c^* := \partial_c f(u_*, c_*)$. The spatially uniform steady-state (10) is unstable if Eq. (13) has any root σ with $\text{Re}(\sigma) > 0$. We refer to D'_* as the motility response since it characterizes how the motility responds to changes in internal concentration. We find that there are two types of instability depending on the sign of D'_* .

Case I: Internal chemical represses motility: The first type of instability occurs when higher internal concentrations reduce motility ($D'_* < 0$), analogous to classic MIPS where

higher cell densities reduce motility through physical interaction.

We derive the following instability criterion by substituting $\sigma = 0$ into (13) and rearranging:

$$\frac{\mathcal{D}'_*}{\mathcal{D}_*} < -\frac{A}{u_*}, \quad (14a)$$

where we define

$$A := \frac{1}{\alpha_0 \rho_* f_c^*} \left(\frac{D_c \pi^2}{L_m^2} + \beta \right) \left(\frac{D_* \pi^2}{L_m^2} + \lambda \right) - 1 > 0. \quad (14b)$$

Here, L_m is the largest side length of the domain, and we use $k = \pi/L_m$ since the longest wavelength mode is always the first to lose stability as \mathcal{D}'_* is decreased from zero (see Sec. B of the Supplemental Material [49]). However, the mode with the largest growth rate, i.e., largest value of $\text{Re}(\sigma)$, typically corresponds to an intermediate wavelength, as shown in Fig. 2.

Equation (14) is the first key result of our Letter. Qualitatively, it states that a spatially uniform population of chemically interacting cells begins to form clusters when the cellular motility (characterized by the diffusion coefficient \mathcal{D}_*) is sufficiently repressed in response to perturbations in the internal concentrations. The constant A , defined in (14b), encodes the required strength of repression in terms of the chemical timescales and genetic structure of the population. The mechanism driving the instability is shown schematically in Fig. 4(a).

A key feature of the instability characterized by (14) is that any of the gene-regulated active motility parameters in (4b) can trigger MIPS, not just the self-propulsion speed $v(u)$. This is in contrast to physical MIPS for which the analog of (14) is given by the criterion [7]:

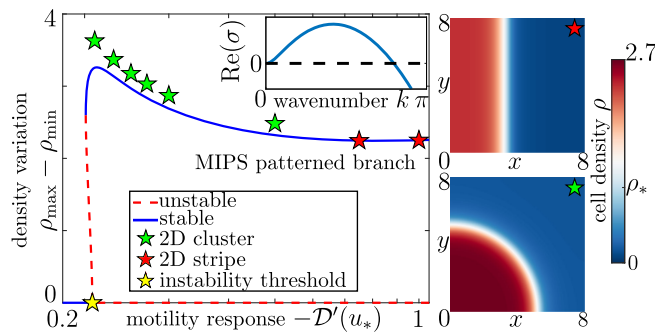


FIG. 2. Bifurcation diagram in one dimension with 2D steady-state stripe (cluster) patterns shown as red (green) stars, respectively (see right panels and video S2 in the Supplemental Material [49]). The trivial branch corresponds to (10) and the bifurcating branch is the 1D MIPS-patterned state [computed from steady-state versions of (4)–(7)]. The bifurcation point (yellow star) is indistinguishable from that predicted from (14). Inset: dispersion relation from linear theory. Parameter values are given in Table S1 of [49].

$$\frac{1}{V} \frac{dV}{d\rho} \Big|_{\rho_*} < -\frac{1}{\rho_*}, \quad (15)$$

where $V(\rho)$ is the effective density-dependent propulsion speed in physical active matter. A similar phenomenon occurs for active (velocity) fluctuations where rotational diffusion affects the onset of MIPS, but is not the underlying cause [53]. The difference between (14) and (15) is that (14) accounts for the timescales of chemical diffusion and gene-regulated motility parameters. As such, we expect that the classical result (15) should be recovered when both the AI concentration and gene-regulatory kinetics equilibrate quickly. We clarify in Secs. B and D of the Supplemental Material [49] that in order to recover (15), the chemical timescales need to be fast not just by comparison to the cell diffusion timescale but also by comparison to the tumbling and reorientation timescales, which necessitates modifying the upscaling procedure used to obtain (4). In this very-fast-chemical-timescale limit, nonconstant rotational diffusion or tumbling frequency cannot cause MIPS, consistent with (15).

The dynamics of the cell density ρ are illustrated in Fig. 1(b), clearly exhibiting MIPS. In Fig. 2 we compute steady-state branches that bifurcate from the uniform state, and show that the bifurcation point predicted by our analysis in (14) agrees well with numerically computed branches. The unstable spatial modes from the dispersion relation $\sigma(k)$, determined from (13), are illustrated in Fig. 2. The spatial mode with the largest growth rate measures the cluster sizes that initially form from the uniform state.

Case II: Internal chemical promotes motility: Surprisingly, our linear stability analysis predicts a new type of instability when higher internal concentrations promote motility ($\mathcal{D}'_* > 0$). Since physical interparticle forces act to reduce motility as density increases, this new instability would not be induced in populations with purely physical interactions. Chemically interacting populations do not have this restriction; GRNs connected to intercellular signalling can increase cell motility directly in, e.g., bacterial swarming where QS regulates flagella assembly [48], and indirectly by, e.g., controlling biosurfactant production [3].

Mathematically, this instability occurs when σ is purely imaginary, i.e., via a Hopf bifurcation. The analog of (14a) for this instability is given by (see Sec. C of the Supplemental Material [49]):

$$\frac{\mathcal{D}'_*}{\mathcal{D}_*} > \frac{B}{u_*}, \quad (16a)$$

where we define

$$B := \frac{\omega_\lambda + \omega}{\omega_0} \left[\frac{(\omega_0 + \omega_\lambda)(\omega_0 + \omega)}{\alpha_0 f_c^* \rho_*} - 1 \right] > 0, \quad (16b)$$

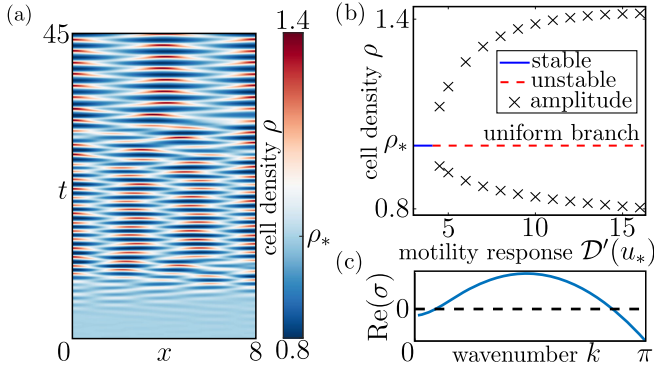


FIG. 3. (a) Oscillatory patterning in one dimension showing the formation of periodic spatiotemporal oscillations resembling standing waves (see also video S3 in [49]). (b) Bifurcation diagram showing the amplitude of density oscillations. (c) Dispersion relation from the linear theory.

$$\omega_j := D_* k^2 + j, \quad \omega := D_c k^2 + \beta. \quad (16c)$$

Equation (16) is the second key result of our Letter. It quantifies the condition under which a uniform population of chemically interacting cells undergoes spatiotemporal density oscillations. Qualitatively, the population becomes unstable when the cellular motility is sufficiently promoted in response to perturbing the internal concentrations. The constant B , defined in (16b), encodes information about the chemical timescales and genetic structure of the population. Similar to the criterion (14), the instability can be triggered if any of the active motility parameters in (4b) are non-constant. In contrast to (14), the longest wavelength mode, in general, is not the first to become unstable, as can be seen by comparing the dispersion relations for the two instabilities in Figs. 2 and 3(c). We show the type of spatiotemporal dynamics arising from this instability in Fig. 3(a). The oscillations tend to a limit cycle resembling a standing wave pattern, which bifurcates from the uniform state as illustrated by Fig. 3(b).

The mechanism driving this new oscillatory instability is an effective time delay between local density fluctuations and changes in motility, illustrated schematically in Fig. 4(b). Oscillatory patterns are known to arise in chemotactic active matter where effective time-delays between changes in density and orientation [21] or chemoattractant [29] drive the instability. Here, the time delay between density and motility is caused by finite timescales in the QS circuit. To understand the mechanism physically, consider a region of locally higher cell density. As the density fluctuation begins to relax, the AI concentration field increases locally in response to the higher density, which leads to locally higher internal concentrations due to the reaction kinetics. Owing to the chemically regulated motility $\mathcal{D}(u)$, the cells with higher internal concentrations experience a higher motility. As the local density returns to the equilibrium value, the locally higher motility persists and the region begins to deplete of

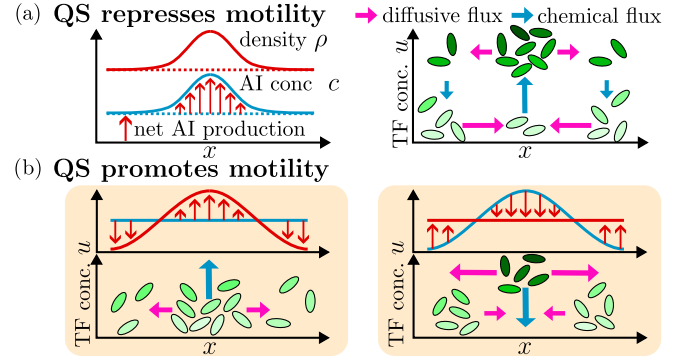


FIG. 4. Schematic illustrations of the instability mechanisms. (a) Small density or AI perturbation from the unstable uniform equilibrium in Case I. (b) Periodic spatiotemporal oscillations in Case II.

cells, thereby forming a region of lower density. This forms the first half of the periodic cycle, with the second half having equivalent reasoning. The oscillations decay if the time delay is too short, which can be seen mathematically by considering the behavior of B as the delay tends to zero, i.e., in the limit of fast chemical timescales (in which $a \sim L \sim \lambda \sim \alpha_0 \sim \beta$ are large). From (16b), it can be shown that $B \rightarrow \infty$ in this limit and hence the criterion (16a) cannot be satisfied, favoring a stable uniform colony.

Our results demonstrate that explicit modeling of gene regulation in cell populations is key to understanding MIPS in living active matter. Our GRN-structured model allows for a direct link between cell-level genetic processes and macroscale pattern formation—in principle, the model can be simplified via an internal mean-field formulation of the governing equations (4)–(7), but this is only quantitatively accurate near the spatially uniform equilibrium (Supplemental Material [49]). More fundamentally, our theory predicts that gene-regulated tumbling frequency alone can cause MIPS, in contrast to classical physical MIPS. Additionally, gene regulation that promotes motility in higher signal concentrations is required for the oscillatory instability (Hopf bifurcation) that we identify here; this instability is absent in systems with purely physical interactions between particles. Our continuum model is appropriate for large cell populations, which are common in many natural [3] and synthetic [5] biological systems. In future work it would be interesting to explore the predictions of agent-based simulations of the microscopic model (1)–(3), (5), and (6), especially for small cell populations.

The code that was used to perform the simulations in this paper is available at Ref. [58]. All data is provided in the paper and in the electronic supplementary material [49].

The authors thank Devi Prasad Panigrahi and Andrew Hazel for helpful discussions. Furthermore, the authors

would like to acknowledge the use of the University of Oxford Advanced Research Computing (ARC) facility in carrying out this work, as well as the UCL Mathematics Department for use of the high performance cluster. W. J. M. R. is grateful for financial support in part from an NSERC PGSD scholarship and in part from Somerville College. M. P. D. is supported by the UK Engineering and Physical Sciences Research Council [EP/W032317/1]. P. P. is supported by a UKRI Future Leaders Fellowship [MR/V022385/1].

*wesley.ridgway@some.ox.ac.uk

†m.dalwadi@ucl.ac.uk

‡philip.pearce@ucl.ac.uk

§chapman@maths.ox.ac.uk

- [1] A. Deutsch, P. Friedl, L. Preziosi, and G. Theraulaz, Multi-scale analysis and modelling of collective migration in biological systems, *Phil. Trans. R. Soc. B* **375**, 20190377 (2020).
- [2] K. Papenfort and B. L. Bassler, Quorum sensing signal-response systems in Gram-negative bacteria, *Nat. Rev. Microbiol.* **14**, 576 (2016).
- [3] R. Daniels, J. Vanderleyden, and J. Michiels, Quorum sensing and swarming migration in bacteria, *FEMS Microbiol. Rev.* **28**, 261 (2004).
- [4] L. E. Weiss, J. P. Badalamenti, L. J. Weaver, A. R. Tascone, P. S. Weiss, T. L. Richard, and P. C. Cirino, Engineering motility as a phenotypic response to LuxI/R-dependent quorum sensing in *Escherichia coli*, *Biotechnol. Bioeng.* **100**, 1251 (2008).
- [5] C. Liu *et al.*, Sequential establishment of stripe patterns in an expanding cell population, *Science* **334**, 238 (2011).
- [6] A. Curatolo, N. Zhou, Y. Zhao, C. Liu, A. Daerr, J. Tailleur, and J. Huang, Cooperative pattern formation in multi-component bacterial systems through reciprocal motility regulation, *Nat. Phys.* **16**, 1152 (2020).
- [7] M. E. Cates and J. Tailleur, Motility-induced phase separation, *Annu. Rev. Condens. Matter Phys.* **6**, 219 (2015).
- [8] B. Partridge and C. F. Lee, Critical motility-induced phase separation belongs to the Ising universality class, *Phys. Rev. Lett.* **123**, 068002 (2019).
- [9] R. A. Simha and S. Ramaswamy, Hydrodynamic fluctuations and instabilities in ordered suspensions of self-propelled particles, *Phys. Rev. Lett.* **89**, 058101 (2002).
- [10] S. Ramaswamy, The mechanics and statistics of active matter, *Annu. Rev. Condens. Matter Phys.* **1**, 323 (2010).
- [11] S. Bhattacharyya and J. M. Yeomans, Phase separation driven by active flows, *Phys. Rev. Lett.* **130**, 238201 (2023).
- [12] T. H. Tan, A. Mietke, J. Li, Y. Chen, H. Higinbotham, P. J. Foster, S. Gokhale, J. Dunkel, and N. Fakhri, Odd dynamics of living chiral crystals, *Nature (London)* **607**, 287 (2022).
- [13] I. Aranson, Bacterial active matter, *Rep. Prog. Phys.* **85**, 076601 (2022).
- [14] S. Bhattacharyya and J. M. Yeomans, Coupling Turing stripes to active flows, *Soft Matter* **17**, 10716 (2021).
- [15] C. Anderson and A. Fernandez-Nieves, Social interactions lead to motility-induced phase separation in fire ants, *Nat. Commun.* **13**, 6710 (2022).
- [16] M. Paoluzzi, M. Leoni, and M. C. Marchetti, Information and motility exchange in collectives of active particles, *Soft Matter* **16**, 6317 (2020).
- [17] G. Courcoubetis, M. S. Gangan, S. Lim, X. Guo, S. Haas, and J. Q. Boedicker, Formation, collective motion, and merging of macroscopic bacterial aggregates, *PLoS Comput. Biol.* **18**, e1009153 (2022).
- [18] S. Saha, R. Golestanian, and S. Ramaswamy, Clusters, asters, and collective oscillations in chemotactic colloids, *Phys. Rev. E* **89**, 062316 (2014).
- [19] A. Gelimson and R. Golestanian, Collective dynamics of dividing chemotactic cells, *Phys. Rev. Lett.* **114**, 028101 (2015).
- [20] R. B. A. Zinati, C. Duclut, S. Mahdisoltani, A. Gambassi, and R. Golestanian, Stochastic dynamics of chemotactic colonies with logistic growth, *Europhys. Lett.* **136**, 50003 (2022).
- [21] B. Liebchen, D. Marenduzzo, I. Pagonabarraga, and M. E. Cates, Clustering and pattern formation in chemorepulsive active colloids, *Phys. Rev. Lett.* **115**, 258301 (2015).
- [22] J. Zhang, R. Alert, J. Yan, N. S. Wingreen, and S. Granick, Active phase separation by turning towards regions of higher density, *Nat. Phys.* **17**, 961 (2021).
- [23] X. Yang, D. Marenduzzo, and M. C. Marchetti, Spiral and never-settling patterns in active systems, *Phys. Rev. E* **89**, 012711 (2014).
- [24] T. Grafke, M. E. Cates, and E. Vanden-Eijnden, Spatiotemporal self-organization of fluctuating bacterial colonies, *Phys. Rev. Lett.* **119**, 188003 (2017).
- [25] N. Gnan and C. Maggi, Critical behavior of quorum-sensing active particles, *Soft Matter* **18**, 7654 (2022).
- [26] C. Abaurrea Velasco, M. Abkenar, G. Gompper, and T. Auth, Collective behavior of self-propelled rods with quorum sensing, *Phys. Rev. E* **98**, 022605 (2018).
- [27] F. Jose, S. K. Anand, and S. P. Singh, Phase separation of an active colloidal suspension *via* quorum-sensing, *Soft Matter* **17**, 3153 (2021).
- [28] A. Ziepkke, I. Maryshev, I. S. Aranson, and E. Frey, Multi-scale organization in communicating active matter, *Nat. Commun.* **13**, 6727 (2022).
- [29] H. Zhao, A. Košmrlj, and S. S. Datta, Chemotactic motility-induced phase separation, *Phys. Rev. Lett.* **131**, 118301 (2023).
- [30] F. R. Macfarlane, T. Lorenzi, and K. J. Painter, The impact of phenotypic heterogeneity on chemotactic self-organisation, *Bull. Math. Biol.* **84**, 143 (2022).
- [31] R. Erban and H. G. Othmer, From individual to collective behavior in bacterial chemotaxis, *SIAM J. Appl. Math.* **65**, 361 (2004).
- [32] S. Yasuda, Effects of internal dynamics on chemotactic aggregation of bacteria, *Phys. Biol.* **18**, 066001 (2021).
- [33] J. Agudo-Canalejo and R. Golestanian, Active phase separation in mixtures of chemically interacting particles, *Phys. Rev. Lett.* **123**, 018101 (2019).
- [34] T. Bhattacharjee, D. B. Amchin, R. Alert, J. A. Ott, and S. S. Datta, Chemotactic smoothing of collective migration, *eLife* **11**, e71226 (2022).
- [35] X. Fu, L.-H. Tang, C. Liu, J.-D. Huang, T. Hwa, and P. Lenz, Stripe formation in bacterial systems with density-suppressed motility, *Phys. Rev. Lett.* **108**, 198102 (2012).

- [36] X. Xue, C. Xue, and M. Tang, The role of intracellular signaling in the stripe formation in engineered *Escherichia coli* populations, *PLoS Comput. Biol.* **14**, e1006178 (2018).
- [37] X. Zhang and N. Mitarai, Finite response time in stripe formation by bacteria with density-suppressed motility, [arXiv:1905.02933](https://arxiv.org/abs/1905.02933).
- [38] M. Rein, N. Heinß, F. Schmid, and T. Speck, Collective behavior of quorum-sensing run-and-tumble particles under confinement, *Phys. Rev. Lett.* **116**, 058102 (2016).
- [39] J. Smith-Roberge, D. Iron, and T. Kolokolnikov, Pattern formation in bacterial colonies with density-dependent diffusion, *Eur. J. Appl. Math.* **30**, 196 (2019).
- [40] A. Fischer, F. Schmid, and T. Speck, Quorum-sensing active particles with discontinuous motility, *Phys. Rev. E* **101**, 012601 (2020).
- [41] T. Bäuerle, A. Fischer, T. Speck, and C. Bechinger, Self-organization of active particles by quorum sensing rules, *Nat. Commun.* **9**, 3232 (2018).
- [42] Y. Fily and M. C. Marchetti, Athermal phase separation of self-propelled particles with no alignment, *Phys. Rev. Lett.* **108**, 235702 (2012).
- [43] J. Stenhammar, A. Tiribocchi, R. J. Allen, D. Marenduzzo, and M. E. Cates, Continuum theory of phase separation kinetics for active Brownian particles, *Phys. Rev. Lett.* **111**, 145702 (2013).
- [44] J. Bialké, H. Löwen, and T. Speck, Microscopic theory for the phase separation of self-propelled repulsive disks, *Europhys. Lett.* **103**, 30008 (2013).
- [45] D. T. Gillespie, A. Hellander, and L. R. Petzold, Perspective: Stochastic algorithms for chemical kinetics, *J. Chem. Phys.* **138**, 170901 (2013).
- [46] S. Tavaddod, M. A. Charsooghi, F. Abdi, H. Khalesifard, and R. Golestanian, Probing passive diffusion of flagellated and deflagellated *Escherichia coli*, *Eur. Phys. J. E* **34**, 1 (2011).
- [47] I. Santra, U. Basu, and S. Sabhapandit, Active Brownian motion with directional reversals, *Phys. Rev. E* **104**, L012601 (2021).
- [48] V. Sperandio, A. G. Torres, and J. B. Kaper, Quorum sensing *Escherichia coli* regulators B and C (QseBC): A novel two-component regulatory system involved in the regulation of flagella and motility by quorum sensing in *E. coli*, *Mol. Microbiol.* **43**, 809 (2002).
- [49] See Supplemental Material at <http://link.aps.org/supplemental/10.1103/PhysRevLett.131.228302> for details regarding the derivation of the governing equations, analysis of the linear stability problem, the Hopf bifurcation criterion, reduction to classical MIPS, numerical methods, and comparison with a mean-field model, which includes Refs. [50–53].
- [50] S. Chapman, J. King, and K. Adams, Exponential asymptotics and Stokes lines in nonlinear ordinary differential equations, *Proc. R. Soc. A* **454**, 2733 (1998).
- [51] T. Gudi, Finite element method for a nonlocal problem of Kirchhoff type, *SIAM J. Numer. Anal.* **50**, 657 (2012).
- [52] oomph-lib: MainPage, <https://oomph-lib.github.io/oomph-lib/doc/html/index.html>. Accessed: 2023-20-02.
- [53] B. Mahault, P. Godara, and R. Golestanian, Emergent organization and polarization due to active fluctuations, *Phys. Rev. Res.* **5**, L022012 (2023).
- [54] J. Bialké, T. Speck, and H. Löwen, Active colloidal suspensions: Clustering and phase behavior, *J. Non-Cryst. Solids* **407**, 367 (2015).
- [55] M. E. Cates and J. Tailleur, When are active Brownian particles and run-and-tumble particles equivalent? Consequences for motility-induced phase separation, *Europhys. Lett.* **101**, 20010 (2013).
- [56] M. P. Dalwadi and P. Pearce, Emergent robustness of bacterial quorum sensing in fluid flow, *Proc. Natl. Acad. Sci. U.S.A.* **118**, e2022312118 (2021).
- [57] M. Heil and A. L. Hazel, oomph-lib—an Object-Oriented Multi-Physics Finite-Element Library, edited by *Fluid-Structure Interaction* H. J. Bungartz and M. Schäfer, Lecture Notes on Computational Science and Engineering Vol. 53 (Springer, New York, 2006), pp. 19–49, [10.1007/3-540-34596-5_2](https://doi.org/10.1007/3-540-34596-5_2).
- [58] <https://github.com/RidgwayWJM/QS-MIPS-Numerics>.